



A MIMO CONTROL STRATEGY FOR THE SOUND QUALITY OF MULTI-HARMONIC DISTURBANCES TRANSMITTED INTO CAVITIES

Jaime A. Mosquera-Sánchez

Leopoldo P. R. de Oliveira

Department of Mechanical Engineering - São Carlos School of Engineering, University of São Paulo

jamosquera@usp.br, leopro@sc.usp.br

Abstract. Active sound quality control in automotive applications is devised to attain predefined sound quality perceptions of the engine noise at the driver's head position. Similarly, it can be desirable guaranteeing the same or even other perceptions of the multi-harmonic disturbance in other locations into the cavity, e.g. at the passengers' positions, which implies taking into account the multiple vibroacoustic transfer paths in the design and implementation of a control algorithm. This paper presents a decentralized, multiple-input/multiple-output strategy for controlling the sound quality of multi-harmonic disturbances, based on the amplitude and relative-phase of their narrowband components. Control effort restrictions are required in the single-input, single-output formulation of the SF-cFxLMS algorithm, core of the proposed adaptive control strategy, for keeping the decentralized systems at suitable levels, thus avoiding cross-action effects that could lead to instabilities, when implemented in a MIMO setup. Computer simulations of the proposed algorithm demonstrate the feasibility of simultaneously reaching predefined sound quality perceptions at two locations inside a fictitious cavity, in terms of the assessment of the obtained time histories and relevant psychoacoustic metrics such as Loudness and Roughness, even though when impulsive occurrences could emerge through the operation of the proposed MIMO system.

Keywords: Active sound quality control, MIMO adaptive control algorithm, multi-harmonic disturbance, sound quality.

1. INTRODUCTION

Active noise control systems in automotive applications are typically implemented for improving the auditory perception of the driver. Concerning the sound quality (SQ) of the engine noise, a number of single-input, single-output (SISO) control algorithms has been reported for improving it, by means of dealing with the amplitude (Rees and Elliott, 2006; Kuo *et al.*, 2008; Oliveira *et al.*, 2010; Jeon *et al.*, 2011) or both amplitude and relative phase of the narrowband components of the multi-harmonic disturbance (Mosquera-Sánchez and Oliveira, 2012). Some researchers (Elliott and Boucher, 1994; Kuo and Morgan, 1996; Cabell and Fuller, 1999; de Diego *et al.*, 2004; Oliveira *et al.*, 2005; Gonzalez *et al.*, 2006; Pasco *et al.*, 2011) have faced the matter of minimizing the overall acoustic and/or vibrational field in enclosures, in terms of reducing or rather equalizing the amplitude of the disturbance (acoustic pressures and/or particle accelerations/velocities), by placing a set of sensors and actuators such that the potential (Kuo and Morgan, 1996) or kinetic energy (Oliveira *et al.*, 2005) can be dealt with. However, previous studies (Mosquera-Sánchez, 2012) have revealed that the active control actions at a specific position can cause -likely undesired- alterations in the acoustic field at other positions inside a cavity.

This paper presents a multiple-input, multiple-output (MIMO) formulation of the Simplified Form, Complex Filtered-X Least Mean Squares (SF-cFxLMS) algorithm (Mosquera-Sánchez and Oliveira, 2012), intended to perform amplitude and/or relative-phase control actions over a set of narrowband components of a multi-harmonic disturbance, at diverse locations inside a cavity. The goal of *independently controlling a number of locations* inside a cavity, rather than controlling of a global acoustic field, implies that the control strategy should be a decentralized one, in which a matrix of coupling factors between multiple error signals (Kuo and Morgan, 1996) can be implemented, which in turn allows reducing computational complexity of the algorithm. Similarly, a quite simple but essential condition regarding positioning of sensor/actuator pairs (SAP) inside an enclosure (Elliott and Boucher, 1994) helps to implement the proposed decentralized control algorithm.

On one hand, when amplification operation modes of the SF-cFxLMS are implemented, the output of the control algorithm is larger than the needed when reduction modes are required. On the other hand, when only relative-phase control is concerned, the adaptive algorithm must increase its output level, even at higher levels than when amplitude modes are implemented, in order to compensate for the amplitude losses due to the result of superpositioning between the disturbance and the shifted relative-phase controller output, as this requirement implies maintaining unaltered the amplitude of the narrowband component being controlled. The increasing levels of control effort would prevent the implementation of the SF-FxLMS algorithm, once the output of the m^{th} control actuator can influence on Q error sensors, which in turn can lead the overall control system into an unstable operation. Therefore, a modification into the SISO algorithm, namely a leaky factor that limits the control effort, must be taken into account when implementing it in a MIMO scheme.

This paper is organized in four sections, where Section 2 presents the derivation of the SISO SF-cFxLMS algorithm and the implementation of the *leaky factor*, aiming at formulating the MIMO adaptive algorithm; Section 3 presents

computer simulations of the proposed decentralized algorithm by using pure-delay transfer paths between the synthesized engine disturbance source and two fictitious locations, which implies use of two sensors and two actuators; and finally Section 4 presents some conclusions about this numerical study.

2. THE SF-cFxLMS ALGORITHM: FORMULATIONS

2.1 SISO Formulation

The original cost function of the SF-cFxLMS algorithm is as follows Mosquera-Sánchez and Oliveira (2012):

$$J_k = E \langle (E'_k[l])^2 \rangle, \quad (1)$$

where $E \langle \cdot \rangle$ denotes the expectation operator; $l = 1, 2, \dots$ is the time index for the block-by-block based operation, once the frequency-domain entities involved in updating the adaptive algorithm are calculated every LT_s s; L is the length of the buffers for performing the Fast Fourier Transform (FFT) operations; k is the bin-index of the FFT, and $T_s = 1/F_s$ is the sampling rate of the system. Equation 1 implies that each of the N Fourier bins has a independent cost function to be minimized, where $N = L$ is the length of the internal FFT. Also, in Eq. 1, the main entity is the pseudoerror of the system $E'[l]$, which is calculated as:

$$E'_k[l] = E_k[l] - \widehat{D}_k[l], \quad (2)$$

where $E_k[l]$ is the frequency-domain error signal defined as follows:

$$e[n] = d[n] - y[n] = d[n] - S(z) (w_{l+1}^T[n] x_N[n]) \Rightarrow E_k[l] = \mathcal{F}(e[n]) = \mathcal{F}([e_0[n] \ e_1[n] \ \dots \ e_{L-1}[n]]^T), \quad (3)$$

and $\widehat{D}_k[l]$ is the estimated disturbance calculated as follows:

$$\widehat{d}[n] = e[n] + \widehat{S}(z) [w_{l+1}^T[n] x_N[n]] \Rightarrow \widehat{D}_k[l] = \mathcal{F}[\widehat{d}[n]] = \mathcal{F}([\widehat{d}_0[n] \ \widehat{d}_1[n] \ \dots \ \widehat{d}_{L-1}[n]]^T), \quad (4)$$

from which the SF-cFxLMS algorithm bases its amplitude and relative-phase control operations, by performing the following calculations:

$$|\widehat{D}_k[l+1]| \equiv g_a \sqrt{\Re(\widehat{D}_k[l])^2 + \Im(\widehat{D}_k[l])^2}; \quad \angle(\widehat{D}_k[l+1]) \equiv \text{mod} \left[\pi g_p + \arctan \left(\frac{\Im(\widehat{D}_k[l])}{\Re(\widehat{D}_k[l])} \right), \pi \right] \quad (5)$$

Since $e[n]$ and $\widehat{d}[n]$ are real-domain signals, Eq. 2 can be conducted by using *truncated* versions of $E_k[l]$ and $\widehat{D}_k[l]$, i.e. the first $N/2 + 1$ Fourier bins can be used for performing Eq. 5 and the subsequent weight updating. It is worth noting that the notation $[l+1]$ in Eq. 3 and Eq. 5 indicates that these calculations are used by the adaptive algorithm in the l^{th} iteration, aiming at yielding the desired amplitude and relative-phase values for the $[l+1]^{\text{th}}$ iteration.

Provided that:

$$f_k = \frac{1}{2\pi} \frac{d\widehat{\phi}_k[l]}{dl}, \quad (6)$$

where $d\widehat{\phi}_k[l] = \angle(\widehat{D}_k[l])$ and f_k is the frequency (in Hertz) of the r^{th} reference signal $x^r[n]$, calculation of Eq. 6 leads to appropriately updating the controller weights by using the *amplitude and relative phase* factors g_a and g_p defined in Eq. 5.

Equation 1 can be calculated *on-line* if the expectation operator is replaced by the instantaneous value of the pseudoerror stated in Eq. 2. Sun and Meng (2006) demonstrate that the gradient estimate given by the minimization of the instantaneous value of the error signal (for the case at hand, the pseudoerror in Eq. 2) can be noisy in non-stationary scenarios, and this noise will propagate into the operation of the adaptive filter as $n \rightarrow \infty$. Hence, weighting of the recent values of the cost function by a *forgetting factor* ρ will smooth the response of the adaptive algorithm, thus improving the algorithm face to *impulsive events*. Mosquera-Sánchez and Oliveira (2012) demonstrate the compatibility of this operation in complex-domain adaptive algorithms by modifying Eq. 1 as follows:

$$\begin{aligned} J_k[l] &= \sum_{\tau=0}^l \rho^{l-\tau} (E'_l[\tau])^2 \\ &= \sum_{\tau=0}^l \left[\Re(E'_l[\tau])^2 + \Im(E'_l[\tau])^2 \right] \end{aligned} \quad (7)$$

Figure 1(b) summarizes the proposed SISO SF-cFxLMS algorithm, i.e. calculations stated in Eq. 1 - 7, as $Q = M = 1$. Calculations for updating the adaptive weights will be presented after discussing some aspects concerning the relative-phase control and the required control output levels for accomplishing such that objective. As the pseudoerror is a complex, frequency-domain entity, the updating algorithm that is derived from Eq. 7 can be classified as a frequency-domain adaptive one.

2.1.1 Control effort and relative-phase requirements

According to Rees and Elliott (2006), by taking the z -transform of Eq. 2 and Eq. 3, an expression for the control effort can be obtained, which will lead to point out some aspects about the behavior of the system when relative-phase control is concerned. In Eq. 3, by making $(w_{l+1}^T[n]x_N[n]) \rightarrow u[n]$, which denotes the output of the control system prior to be passed by through the secondary path, we can obtain the optimum control effort when the pseudoerror is completely reduced ($e'[n] = 0$), hence:

$$\begin{aligned} E(z) &= D(z) - S(z)U(z), \\ E'(z) &= E(z) - \widehat{D}(z) \Rightarrow E'(z) = 0 \rightarrow E(z) = \widehat{D}(z), \\ U_{opt}(z) &= \frac{\widehat{D}(z) - D(z)}{S(z)} \end{aligned} \quad (8)$$

In Eq. 8 we can take the discrete Fourier transform, i.e. $z = j\omega T$, thus leading to write (Rees and Elliott, 2006): $D(z) = De^{j\phi_d}$; $\widehat{D}(z) = \widehat{D}e^{j\phi_{\widehat{d}}}$; $U_{opt}(z) = U_{opt}$ and $S(z) = S$ as the secondary path dynamics is assumed as time-invariant, and the other signals are assumed as wide-sense stationary. The control effort is proportional to the square of the output of the controller, hence:

$$U_{opt}^2 = \frac{(\widehat{D}e^{j\phi_{\widehat{d}}} - De^{j\phi_d})^2}{S^2} = \frac{\widehat{D}^2 + D^2 - 2\widehat{D}D\cos(\phi_{\widehat{d}} - \phi_d)}{S^2} \quad (9)$$

From Eq. 9, it can be observed that, as $(\phi_{\widehat{d}} - \phi_d) \rightarrow \pm\pi$, $U_{opt}^2 \rightarrow \left(\frac{\widehat{D}+D}{S}\right)^2$ which indicates the maximum allowable control effort. Provided that $\widehat{S}(z) = S(z)$ and no amplitude operation is applied, the output of the system will be the narrowband component itself, only with its shifted relative phase. On the other hand, as $(\phi_{\widehat{d}} - \phi_d) \rightarrow 0$, $U_{opt}^2 \rightarrow \left(\frac{\widehat{D}-D}{S}\right)^2$, which indicates the minimum allowable control effort, which happens when both the disturbance and its estimate are aligned in relative-phase.

2.1.2 Proposed SISO adaptive algorithm

Since the condition of maximum effort can excite nonlinearities in the actuators, it arises a need of constraining the output of the system to suitable levels. Furthermore, in view of implementing a MIMO strategy for taking advantage of the capabilities of the SF-cFxLMS algorithm, it is mandatory to *constrain* the controller output to suitable levels such that the cross-actions among diverse decentralized systems do not interfere with each other, at the expenses of reducing performance of the algorithm. This goal can be accomplished by imposing a restriction over the output of the controller, which forces the original cost function of the SF-cFxLMS algorithm to be:

$$J_k[l] = \sum_{\tau=0}^l \rho_k^{l-\tau} (E'_k[\tau])^2 + \Psi (U_k[\tau])^2 = \sum_{\tau=0}^l \rho_k^{l-\tau} (E'_k[\tau])^2 + \Psi (W_k[\tau])^2, \quad (10)$$

where $U_k[l]$ is the frequency-domain output $u[n]$ of the control algorithm, and Ψ is a $L \times L$ diagonal weighting matrix with elements $\psi_k \equiv (1 - \mu_k \delta_k)$ being the weightings of the secondary signal power $u^2[n]$.

Use of the traditional steepest descent algorithm by minimizing Eq. 10 with respect to the real and imaginary parts of the adaptive weights leads to write:

$$\begin{aligned} \gamma_k[l] &= \sum_{\tau=0}^l \rho_k^{l-\tau} (E'_k[\tau] X'_{kN}[\tau]), \\ W_k[l+1] &= \psi_k W_k[l] + 2\mu_k \gamma_k[l] \end{aligned} \quad (11)$$

In Eq. 11, X'_{kN} stands for the complex conjugate of the filtered reference, which is initially normalized in the time domain as follows:

$$x_N[n] = |N(\omega)| x[n] \Rightarrow x'_N[n] = x_N[n] * \widehat{S}(z), \quad (12)$$

thereafter, a Fourier transform is performed over $x'_N[n]$ as follows:

$$X'_N[l] = \mathcal{F}(x'_N[n]) = \mathcal{F}([x'_0[n] \quad x'_1[n] \quad \cdots \quad x'_{L-1}[n]]^T) \quad (13)$$

Note that the Fourier transform is performed only after filtering of the normalized reference by the secondary path estimate $\widehat{S}(z)$. The normalizing procedure is performed by using the NEX-LMS approach (Oliveira *et al.*, 2010), defined as follows:

$$\frac{0.01}{\widehat{S}(\omega)} \leq N(\omega) \leq \frac{0.1}{\widehat{S}(\omega)} \quad (14)$$

After performing some algebraic manipulations, we can arrive at a practical implementation of Eq. 11 such as:

$$\begin{aligned}\gamma_k[l] &= \rho_k \gamma_k[l-1] + E'_k[l] X'_{kN}{}^*[l], \\ W_k[l+1] &= \psi_k W_k[l] + 2\mu_k \gamma_k[l],\end{aligned}\quad (15)$$

which constitutes the proposed constrained SISO SF-cFxLMS adaptive algorithm. For numerical stability of the algorithm, $\rho \in [0, 1)$ and $\delta_k \in (0, \infty)$. As long as $\delta_k = 0$, the algorithm reduces to the original SF-cFxLMS algorithm, whereas that $\rho = 0$, the algorithm reduces to the frequency-domain FxLMS algorithm, provided that $\delta_k = 0$.

2.2 MIMO Formulation

In this paper we are interested in the active control of the acoustic field at Q points inside a cavity. A set of R narrowband components can be settled as the control objectives, which could equal the entire O engine orders of the primary disturbance. Thus, by using the knowledge of the rotating speed of the engine and the engine orders requiring control, the control algorithm is able to synthesize a set of reference signals that will be added together in order to elaborate M reference signals:

$$x_m[n] = \sum_{i=1}^R \sin[2\pi\omega_i n] \Rightarrow \mathbf{X}[l] = [x_1[l] \quad x_2[l] \quad \cdots \quad x_M[l]]^T, \quad (16)$$

which it is supposed to be highly correlated with the primary disturbance.

The control algorithm measures Q error signals:

$$\mathbf{E}[l] = [e_1[l] \quad e_2[l] \quad \cdots \quad e_Q[l]]^T \quad (17)$$

Each of the q^{th} error signals are derived from the linear superposition of the primary disturbance $d[n]$, as stated in Eq. 3, measured by Q error sensors:

$$\mathbf{D}[l] = [d_1[l] \quad d_2[l] \quad \cdots \quad d_Q[l]]^T, \quad (18)$$

and the Q filtered control output signals by the secondary transfer paths:

$$\mathbf{Y}[l] = [y_1[l] \quad y_2[l] \quad \cdots \quad y_Q[l]]^T \quad (19)$$

After processing of the error and reference signals, the control algorithm generates M signals to be superimposed to the primary disturbance:

$$\mathbf{U}[l] = [u_1[l] \quad u_2[l] \quad \cdots \quad u_M[l]]^T, \quad (20)$$

to be passed through the control loops, for generating the control signals by using the M actuators in the system. Note that each of the u^{th} control signals are derived from filtering the m^{th} reference signal through the m^{th} adaptive filter:

$$\mathbf{W}[l] = [w_1^T[l] \quad w_2^T[l] \quad \cdots \quad w_M^T[l]]^T, \quad (21)$$

such that:

$$\mathbf{U}[l] = \mathbf{X}_N^T[l] \mathbf{W}[l], \quad (22)$$

where:

$$\mathbf{X}_N[l] = \left| \mathbf{N}_m^T(\omega) \right| \mathbf{X}[l] = [x_1^N[l] \quad x_2^N[l] \quad \cdots \quad x_M^N[l]]^T \quad (23)$$

The m^{th} reference signal in Eq. 23 is normalized by using a gain vector $\mathbf{N} = [N_1(\omega), N_2(\omega), \dots, N_M(\omega)]^T$, in which each of the elements is given by the normalization strategy stated in Eq. 14. Since only an estimate of the secondary paths is generally available, the normalization procedure can be realized by taking the main diagonal elements of the $Q \times M$ secondary path estimate matrix $\hat{\mathbf{S}}(z)$:

$$\mathbf{S}(z) \equiv \begin{bmatrix} S_{11}(z) & S_{12}(z) & \cdots & S_{1M}(z) \\ S_{21}(z) & S_{22}(z) & \cdots & S_{2M}(z) \\ \vdots & \vdots & \ddots & \vdots \\ S_{Q1}(z) & S_{Q1}(z) & \cdots & S_{QM}(z) \end{bmatrix} \approx \hat{\mathbf{S}}(z) \equiv \begin{bmatrix} \hat{S}_{11}(z) & \hat{S}_{12}(z) & \cdots & \hat{S}_{1M}(z) \\ \hat{S}_{21}(z) & \hat{S}_{22}(z) & \cdots & \hat{S}_{2M}(z) \\ \vdots & \vdots & \ddots & \vdots \\ \hat{S}_{Q1}(z) & \hat{S}_{Q1}(z) & \cdots & \hat{S}_{QM}(z) \end{bmatrix}, \quad (24)$$

where $S_{qm}(z)$ represents the actual secondary path dynamics from the m^{th} control actuator to the q^{th} error sensor and $\hat{S}_{qm}(z)$ represents the estimated secondary path in a finite impulse response (FIR) form. In Eq. 24, provided that $q = m$,

i.e. the main diagonal elements, $S_{qm}(z) \approx \hat{S}_{qm}(z)$ represent the secondary path estimate between the m^{th} actuator and its corresponding q^{th} actuator, which can be extracted for conducting the normalization procedures for the m^{th} reference signal.

The q^{th} control signal at the q^{th} error sensor results from the individual contributions of the M control signals, and it can be written as follows (Kuo and Morgan, 1996):

$$y_q[n] = \sum_{m=1}^M S_{qm}[n] * u_m[n] = (S_{q1} * u_1[n]) + (S_{q2} * u_1[n]) + \dots + (S_{qM} * u_M[n]) \quad (25)$$

Note that, by virtue of the requirement in Eq. 23 for normalizing the reference signals, the number of error sensors should be equal or greater than the number of actuators in the system.

Figure 1(a) shows the proposed decentralized MIMO SF-cFxLMS algorithm. In Fig. 1(a) it is assumed that $Q = M$, which implies that the q^{th} sensor is controlled by its respective m^{th} actuator. Also, as *spacial-independent* control is desired, summation of the Q error signals for updating the m^{th} set of adaptive weights is not necessary. Next subsection is devoted to derive the adaptive decentralized algorithm that includes controller effort constraints and a robust gradient estimate of the cost function.

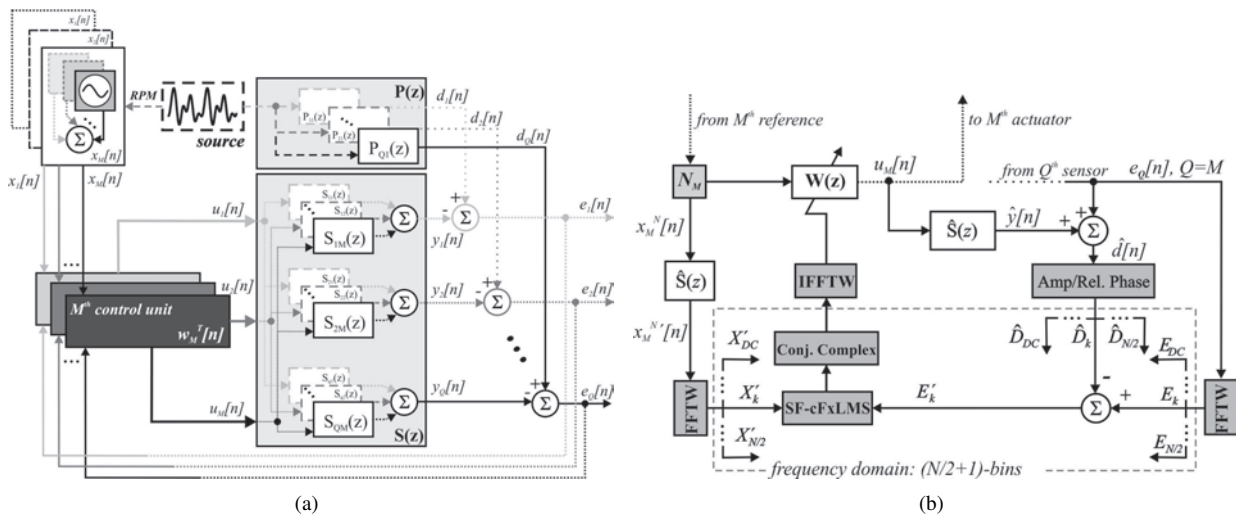


Figure 1. Decentralized MIMO SF-cFxLMS algorithm: (a) Control Scheme; (b) Detail of the M^{th} -channel

Proposed MIMO adaptive algorithm

From the definition of the pseudoerror of the SISO algorithm (Eq. 2), it can be observed that all the calculations for finding the q^{th} pseudoerror in the MIMO control strategy can be conducted by using the q^{th} error signal and the q^{th} estimate of the primary disturbance, which can be calculated as follows:

$$\hat{d}_q[n] = e_q[n] + \hat{S}_{qq}(z) \sum_{m=1}^M [w_m^T[n] x_m^N[n]] \Rightarrow \hat{\mathbf{D}}[l] = \mathcal{F}[\hat{d}_q[n]] = \mathcal{F}([\hat{d}_0[n] \quad \hat{d}_1[n] \quad \dots \quad \hat{d}_Q[n]]^T), \quad (26)$$

An expression for the q^{th} pseudoerror can be derived by taking Eq. 2, Eq. 17 and Eq. 26 as follows:

$$E'_q[l] = E_q[l] - \hat{D}_q[l] \Rightarrow \mathbf{E}'[l] = [E'_1[n] \quad E'_2[n] \quad \dots \quad E'_Q[n]]^T \quad (27)$$

Equation 27 can be used for deriving the frequency-dependent, MIMO cost function of the system to be minimized, as follows:

$$J_k = \sum_{q=1}^Q E \left\langle \left(E'_{(k,q)}[l] \right)^2 \right\rangle \quad (28)$$

As with the SISO case, the expectation operator can be changed by the instantaneous value of the pseudoerror and further restrictions over the controller outputs can be included. Also, a forgetting factor can be used for replacing the instantaneous value-based cost function by a robust measure, thus improving the gradient estimate of the cost function. Hence, the proposed cost function for the constrained MIMO SF-cFxLMS algorithm is as follows:

$$J_k[l] = \sum_{q=1}^Q \left(\sum_{\tau=0}^l \rho_k^{l-\tau} \left(E'_{(k,q)}[\tau] \right)^2 + \Psi \left(W_{(k,q)}[\tau] \right)^2 \right)$$

$$= \sum_{q=1}^Q \left(\sum_{\tau=0}^l \rho_k^{l-\tau} \left(E'_{(k,q)}[\tau] E'_{(k,q)}[\tau] \right) + W_{(k,q)}^*[\tau] \Psi W_{(k,q)}[\tau] \right) \quad (29)$$

By minimizing Eq. 29 with respect to the m^{th} set of complex-domain adaptive weights W , for a specific k^{th} frequency, we arrive at:

$$W_k^m[l+1] = \psi_k W_k^m[l] + 2\mu_k \sum_{q=1}^Q \gamma_k^q[l], \quad (30)$$

where $\psi_k \equiv 1 - \mu_k \delta_k$, as defined for the SISO control algorithm and:

$$\gamma_k^q[l] = \sum_{\tau=0}^l \rho_k^{l-\tau} \left(E'_{(k,q)}[\tau] X'_{(k,m)}^*[\tau] \right) \quad (31)$$

Since we are interested in guaranteeing different auditory conditions for each of the Q error sensor's positions, we can employ M independent weights for controlling the influence of the Q error signals on each of the M adaptive filters (Kuo and Morgan, 1996), as follows:

$$\mathbf{V}_m \equiv \begin{bmatrix} v_{m1} & 0 & \dots & 0 \\ 0 & v_{m2} & \dots & 0 \\ \vdots & \vdots & \ddots & \vdots \\ 0 & 0 & \dots & v_{mQ} \end{bmatrix}, m = 1, 2, \dots, M, \quad (32)$$

which allows rewriting of Eq. 31 as a function of the redefined pseudoerror $E'_{(k,mq)}[l] \equiv v_{mq} E'_{(k,q)}[l]$:

$$\gamma_k^q[l] = \sum_{\tau=0}^l \rho_k^{l-\tau} \left(E'_{(k,mq)}[\tau] X'_{(k,m)}^*[\tau] \right) \quad (33)$$

The case when $M = Q$ and $v_{mq} = 1$ only when $m = q$ results in the decentralized constrained MIMO SF-cFxLMS algorithm, proposed for independently controlling the sound quality of a multi-harmonic disturbance at Q diverse positions. A stability condition has been derived by Elliott and Boucher (1994) for a $1 \times 2 \times 2$ MIMO system, from which it was concluded that the distance between a specific control actuator and its corresponding error sensor (d_c) must be less than the distance among these control actuator and the other error sensors (d_u), i.e. $d_u > d_c$. This stability condition concerns the positioning of the sensor/actuator pair (SAP) in the enclosure being controlled, and it is generalizable to any amount of sensor actuators provided that the system is fully-determined, i.e. $Q = M$.

Further algebraic manipulation of Eq. 33 and once that $v_{mq} = 1$ only when $m = q$, the constrained, decentralized MIMO SF-cFxLMS algorithm is hence formulated as follows:

$$\begin{aligned} \gamma_k^m[l] &= \rho_k^m \gamma_k^m[l-1] + E'_{(k,mq)}[l] X'_{(k,m)}^*[l], \\ W_k^m[l+1] &= \psi_k W_k^m[l] + 2\mu_k \gamma_k^m[l], \end{aligned} \quad (34)$$

as only one q^{th} error signal has remained from applying the weight matrix \mathbf{V}_m by using the condition $v_{mq} = 1$ when $m = q$. Note that the remaining q^{th} error signal corresponds to the m^{th} actuator that is intended to control the q^{th} position. This decentralized MIMO formulation achieves a great reduction in the computational complexity of the system, compared with pure time-domain approaches such as the MIMO ANE proposed by Kuo and Morgan (1996) and the common-error, multiple-frequency ANE proposed by Gonzalez *et al.* (2006). The computational burden of the proposed decentralized constrained MIMO SF-cFxLMS algorithm is comparable with principal component algorithms such as the proposed by Cabell and Fuller (1999) and Pasco *et al.* (2011), with the advantage of offering robustness face to slight frequency drifts of the primary disturbance, once that the proposed algorithm uses a *non-truncated* version of the secondary path dynamics for filtering the reference signal in a m^{th} channel, at the expenses of increasing the computational burden of the system.

3. COMPUTER SIMULATIONS

This section is devoted to showing computer simulations of the proposed constrained MIMO SF-cFxLMS by using pure-delay transfer paths and a synthesized stationary engine sound obtained from the *LMS.VirtualCarSound* software. Since automotive applications are concerned, we have performed simulations for two locations inside a fictitious cavity: driver's and passenger's positions, which involves use of two error sensors. Also, as local control is desired, two actuators are positioned in the system, which results in $R \times 2 \times 2$ MIMO systems, where R is the number of reference signals used for each of the two simulation scenarios to be shown next. All the simulations and psychoacoustical analyses were performed on *Simulink* and *MATLAB*, respectively. The control algorithms are ran by using a sample rate of 2048 Hz. All

the simulation scenarios are contaminated with white noise of zero mean and variance $10e^{-06} Pa^2$ during 5 s. Results are consolidated after 100 independent runs of each amplitude/relative-phase condition at simultaneously both positions.

Two simulation scenarios are presented in this Section: (i) Active control of two different narrowband components: 2.0 and 8.0 engine orders at the driver's position, and 4.0 and 10.0 engine orders at the passenger's position (two $2 \times 2 \times 2$ decentralized MIMO system) and (ii) Simultaneous active control of four narrowband components at both driver's and passenger's positions: 2.0, 4.0, 8.0 and 10.0 engine orders (a couple of $4 \times 2 \times 2$ decentralized MIMO systems). Each of the above-mentioned simulation scenarios includes both amplitude and relative phase control and the corresponding SQ analyses. A third simulation scenario (Scenario 3.2.1) is derived from the second one, aiming at demonstrating the use of the forgetting factor ρ face to a deliberately inserted impulsive event after the first two seconds of operation, while trying to control the amplitudes of the set of narrowband components described in Scenario 2, at both positions.

Transfer Paths

The primary transfer paths, i.e. the transfer paths from the disturbance source to the error sensors are modelled as a pure-delay, finite impulse response (FIR) transfer functions, formulated as follows:

$$\begin{aligned} P_1(z) &= z^{-15} - 0.3z^{-16} + 0.2z^{-17} \\ P_2(z) &= z^{-14} + z^{-15} - 0.3z^{-16} + 0.2z^{-17} \end{aligned} \quad (35)$$

As with the primary paths, the secondary paths are also modelled as a pure-delay, FIR transfer functions, as follows:

$$\mathbf{S}(z) = \begin{bmatrix} S_{11}(z) = z^{-7} + 1.5z^{-8} - z^{-9} & S_{21}(z) = z^{-10} + 1.5z^{-11} - z^{-12} \\ S_{12}(z) = -0.5z^{-5} + z^{-10} + 1.5z^{-11} - z^{-12} & S_{22}(z) = -0.5z^{-2} + z^{-7} + 1.5z^{-8} - z^{-9} \end{bmatrix}, \quad (36)$$

where $S_{qm}(z)$ is as defined in Eq. 23. Both the primary and secondary paths are modified versions of the ones used by Sun and Meng (2006). For all the simulations, it is assumed that $\hat{\mathbf{S}}(z) = \mathbf{S}(z)$.

Figure 2 shows the frequency-domain responses of the primary paths, whereas that Fig. 3 shows the frequency-domain response of the secondary paths. In Fig. 2 the absolute phase information gives the idea of the error sensors' position with respect of the disturbance source; once that this parameter is approximately the same for both transfer paths, it can be inferred that both sensors are at the same physical distance from the disturbance source. A similar analysis can be performed from the absolute phase data of the secondary paths plotted in Fig. 3. Note that S_{11} and S_{22} have the same absolute phase, whereas that the same happens for S_{12} and S_{21} , which indicates that the m^{th} actuator is near the q^{th} corresponding error sensor. This fact also indicates that every actuator is far from each other, in order to reduce the cross-coupling between them (Kuo and Morgan, 1996).

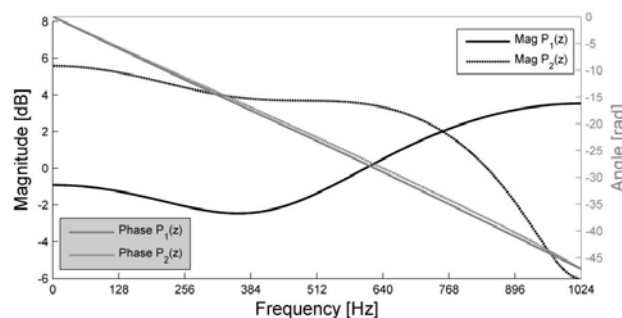


Figure 2. Primary paths (frequency-domain)

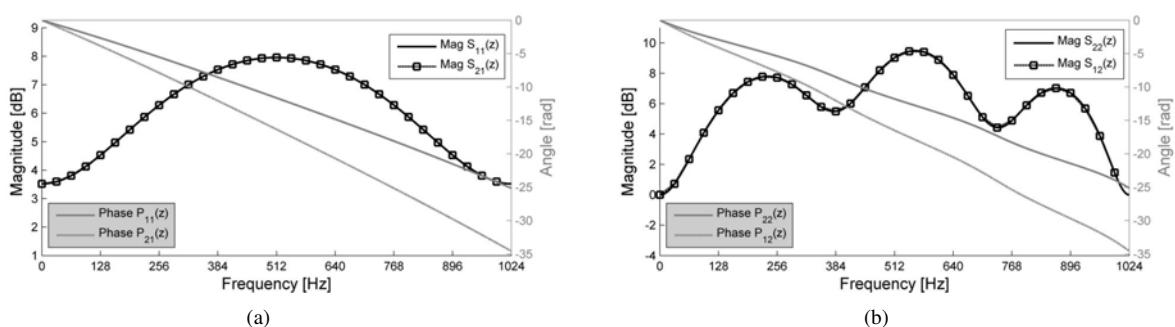


Figure 3. Secondary paths (frequency-domain): (a) $S_{L1}(z)$; (b) $S_{L2}(z)$

Synthesized Engine Noise

From a synthesized run-up noise of an internal combustion engine, we have chosen a low-speed engine regime (1920 RPM) for demonstrating the implementation of the proposed control algorithm. A number of control actions is applied over the engine noise and the results are analyzed in terms of two time-domain SQ metrics such as Loudness model (Fastl and Zwicker, 2007) and Roughness model (Daniel and Weber, 1997). Loudness is assessed once that the amplitude control actions are performed aiming at controlling this SQ characteristic. Roughness is also evaluated, as this psychoacoustical phenomenon is sensitive to changes in the amplitude and relative phase of a set of nearby narrowband components that falls into a critical band (Pressnitzer and McAdams, 1999; Janssens *et al.*, 2007). The selected disturbance exhibits a non-controlled Loudness of 2.26 sone and a Roughness of 0.02 asper at the driver's position, and non-controlled Loudness and Roughness of 3.79 sone and 0.02 asper, respectively, at the passenger's position.

3.1 Scenario One

We have implemented the active control of the amplitude and relative-phase of both the 2.0 and 8.0 engine orders at the driver's position, and the results are plotted in Fig. 4. The control actions at the driver's position are highlighted through red lines, whereas the narrowband components being simultaneously controlled at the passenger's position, i.e. 4.0 and 10.0 engine orders are highlighted through black lines. Operation ranges of 78.55 dB SPL for the 2.0 engine order and of 43.24 dB SPL for the 8.0 engine order were attained after two seconds of continuous controller operation (see numerical results in Tab. 1). Also, wide relative-phase shiftings for the mentioned components between $[-\pi, \pi]$ were attained, without distorting other neighbor narrowband components.

The performed amplitude control actions over the 4.0 and 10.0 engine orders at the passenger's position did not alter their own values at the driver's position, as it can be evidenced through the plotted black lines in Fig. 4(a), which are *approximately* straight across the amplitude operation modes. Operation ranges of 54.8 dB SPL for the 4.0 engine order and of 55.38 dB SPL for the 10.0 engine order were attained. Also, wide relative-phase shiftings for the mentioned components between $[-\pi, \pi]$ were attained. Moreover, it appears that, while the relative-phase of the 10.0 engine order maintained its value across the relative-phase operation modes at the driver's position (see Fig. 4(b)), the same did not hold for the 4.0 engine order, once that the relative-phase of this component showed strong variations.

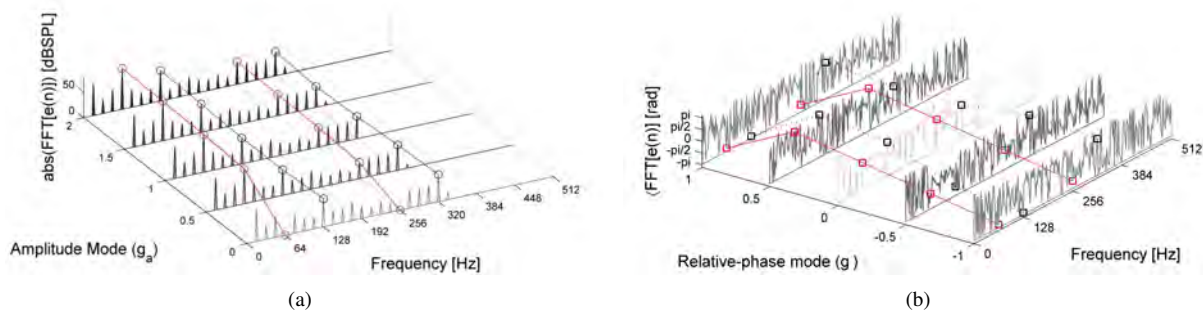


Figure 4. Control actions over the 2.0 and 8.0 integer orders of the engine disturbance when rotating at 1920 RPM, at the driver's position: (a) Amplitude modes; (b) Relative-phase modes

The implemented control actions for the passenger did not distort the neighbor components, nor the taken control actions at the driver's position distorted the other components at the passenger's position. This fact can be evidenced by visually comparing the black lines over the narrowband components being controlled both in Fig. 4 and Fig. 5. It is worth noting that the relative-phase of the components being controlled at the driver's position remained unchanged at the passenger's position.

SQ Analysis

Table 1 numerically illustrates the effect on the SQ of controlling the amplitudes at both the driver and passenger positions. As expected, controlling of the amplitudes directly influenced the perceived Loudness of the disturbance. Hence, Loudness ranges of 1.38 sone at the driver's position and 1.83 sone at the passenger's position were attained. The perceived Roughness remained approximately the same for most of the control operations at both positions, as expected, except the case of total reduction, i.e. $g_a = 0.0$ of the targeted components at the passenger's position, where it was observed a slight but unperceivable increase of the metric. Once that the targeted engine orders could play some role on the generation of Roughness, their reduction could also originate the emergence of other important interactions among the remaining integer/half-integer engine orders of the disturbance, which possibly led to the increase of the auditory phenomenon.

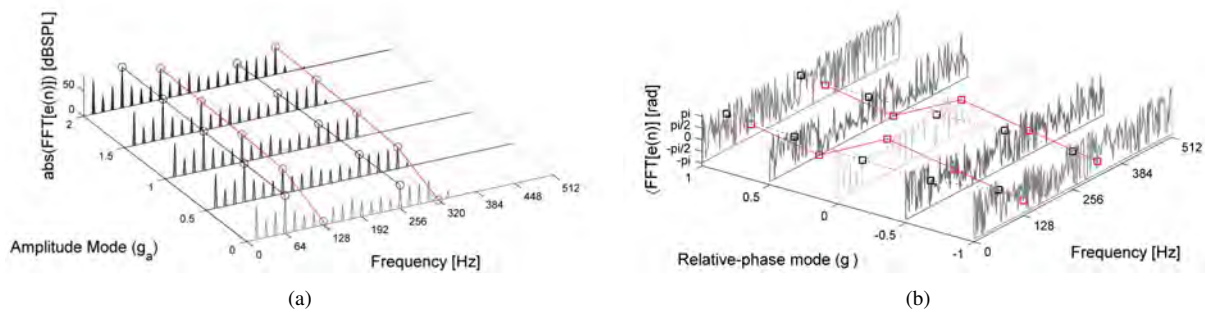


Figure 5. Control actions over the 4.0 and 10.0 integer orders of the engine disturbance when rotating at 1920 RPM, at the passenger's position: (a) Amplitude modes; (b) Relative-phase modes

Table 1. Amplitude modes and Sound Quality assessment for Example 1

| Position | Ord. | $g_a = 2.0$ | | | | $g_a = 1.5$ | | | $g_a = 1.0$ | | | $g_a = 0.5$ | | | $g_a = 0.0$ | | |
|-----------|------|-------------|-------|-------|-------|-------------|-------|-------|-------------|-------|-------|-------------|-------|-------|-------------|-------|-------|
| | | dB | sones | asper | | dB | sones | asper |
| Driver | 2.0 | 78.55 | 3.40 | 0.02 | 76.05 | 2.68 | 0.02 | 72.53 | 2.26 | 0.02 | 66.5 | 2.00 | 0.03 | 0.00 | 2.02 | 0.01 | |
| | 8.0 | 43.24 | | | 40.71 | | | 37.19 | | | 31.28 | | | 0.00 | | | |
| Passenger | 4.0 | 61.98 | 4.84 | 0.02 | 59.48 | 4.31 | 0.02 | 55.96 | 3.79 | 0.02 | 49.92 | 3.30 | 0.03 | 7.182 | 3.01 | 0.05 | |
| | 10.0 | 55.38 | | | 52.85 | | | 49.33 | | | 43.26 | | | 0.00 | | | |

On the other hand, Tab. 2 shows the numerical results of the relative-phase control actions at both the driver and passenger positions, and their influence on both Loudness and Roughness. Ranges of 0.03 asper at the driver's position and 0.09 asper at the passenger's position were attained. Comparing these results with Tab. 1, it can be observed that the relative-phase actions have more influence than the amplitude actions over this auditory phenomenon.

Table 2. Relative-phase modes and Sound Quality assessment for Example 1

| Position | Ord. | $g_p = 1.0$ | | | $g_p = 0.5$ | | | $g_p = 0.0$ | | | $g_p = -0.5$ | | | $g_p = -1.0$ | | |
|-----------|------|-------------|-------|-------|-------------|-------|-------|-------------|-------|-------|--------------|-------|-------|--------------|-------|-------|
| | | rad | sones | asper | rad | sones | asper | rad | sones | asper | rad | sones | asper | rad | sones | asper |
| Driver | 2.0 | -2.68 | 3.65 | 0.05 | 2.032 | 3.02 | 0.03 | 0.46 | 2.26 | 0.02 | -1.11 | 3.34 | 0.04 | -2.68 | 3.65 | 0.05 |
| | 8.0 | -2.15 | | | 2.57 | | | 0.98 | | | -0.56 | | | -2.14 | | |
| Passenger | 4.0 | -1.48 | 3.32 | 0.09 | -3.04 | 2.67 | 0.11 | 1.67 | 3.79 | 0.02 | 0.10 | 4.08 | 0.04 | -1.48 | 3.32 | 0.09 |
| | 10.0 | -1.47 | | | -3.05 | | | 1.66 | | | 0.09 | | | -1.48 | | |

3.2 Scenario Two

The second simulation scenario is intended to simultaneously controlling amplitude *or* relative phase of the 2.0, 4.0, 8.0 and 10.0 engine orders at both the driver and passenger positions. For improving stability of the system while reducing the cross-action effects between the two SAP, it is necessary including of the constraining factor " δ ", which results in the implementation of the proposed constrained MIMO SF-cFxLMS algorithm. Results of the control actions at the driver's position (both amplitude and relative-phase operation modes) are shown in Fig. 6, whereas the control actions at the passenger's position are plotted in Fig. 7. The targeted engine orders are highlighted through black lines at both figures.

Table 3. δ -factors for the SF-cFxLMS operation modes

| Position | Engine Order | Amplitude Modes (g_a) | | | | | Relative-phase Modes (g_p) | | | | |
|-----------|--------------|---------------------------|------|-----|------|------|--------------------------------|------|-----|------|------|
| | | 2.0 | 1.5 | 1.0 | 0.5 | 0.0 | 1.0 | 0.5 | 0.0 | -0.5 | -1.0 |
| Driver | 2.0 | 60.0 | 60.0 | 0.0 | 60.0 | 60.0 | 20.0 | 30.0 | 0.0 | 30.0 | 20.0 |
| | 4.0 | 60.0 | 60.0 | 0.0 | 60.0 | 60.0 | 40.0 | 40.0 | 0.0 | 40.0 | 40.0 |
| | 8.0 | 10.0 | 10.0 | 0.0 | 10.0 | 10.0 | 20.0 | 6.0 | 0.0 | 6.0 | 20.0 |
| | 10.0 | 5.0 | 5.0 | 0.0 | 5.0 | 5.0 | 20.0 | 5.0 | 0.0 | 5.0 | 20.0 |
| Passenger | 2.0 | 40.0 | 40.0 | 0.0 | 40.0 | 40.0 | 50.0 | 10.0 | 0.0 | 10.0 | 50.0 |
| | 4.0 | 30.0 | 30.0 | 0.0 | 30.0 | 30.0 | 15.0 | 10.0 | 0.0 | 10.0 | 15.0 |
| | 8.0 | 5.0 | 5.0 | 0.0 | 5.0 | 5.0 | 20.0 | 20.0 | 0.0 | 20.0 | 20.0 |
| | 10.0 | 10.0 | 10.0 | 0.0 | 10.0 | 10.0 | 20.0 | 30.0 | 0.0 | 30.0 | 20.0 |

The MIMO SF-cFxLMS algorithm is implemented by using the set of δ -factors reported in Tab. 3. It is worth noting that the δ -factors in Tab. 3 were given for guaranteeing the best auditory condition for the driver. It can be evidenced from Fig. 6 that the amplitude of the 2.0 engine order is the largest in the disturbance, which implies that larger control efforts will be necessary in order to achieve reductions and/or amplifications, at a specific position. Hence, since large control outputs can interfere other outputs in the system, it is necessary to implement large constrain values in order to reduce the

cross action between the driver and passenger positions. Note that $\delta = 0.0$ for $g_a = 1.0$ and $g_p = 0.0$, as they are the inactive amplitude and relative-phase control modes, respectively.

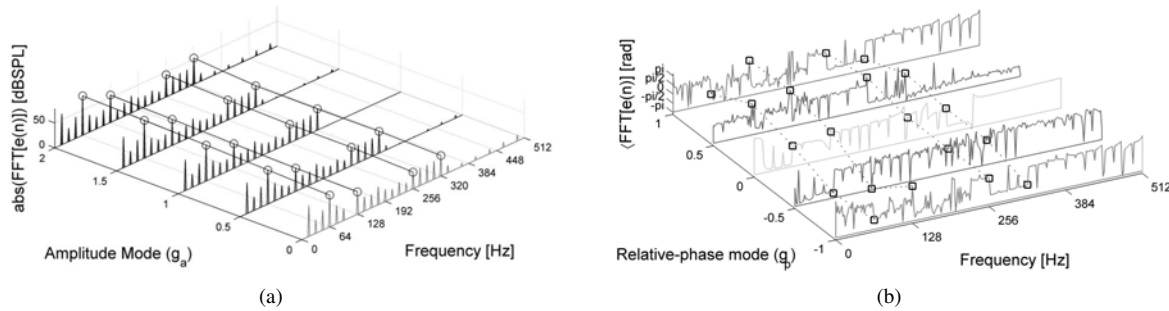


Figure 6. Control actions over the 2.0, 4.0, 8.0 and 10.0 integer orders of the engine disturbance when rotating at 1920 RPM, at the driver's position: (a) Amplitude modes; (b) Relative-phase modes

By comparing Fig. 6(a) with the results shown in Fig. 4(a), i.e. amplitude modes at the driver's position, it can be shown that the maximum achieved reduction levels in Scenario One for the 2.0 and 8.0 engine orders were drastically reduced, as a consequence of implementing control effort constrainings (see numerical results in Tab. 1 and Tab. 4). In a similar manner, when comparing Fig. 7(a) and Fig. 5(a), i.e. the results at the passenger's position, it can be evidenced that the maximum achieved reductions were significantly reduced (see numerical results in Tab. 1 and Tab. 4).

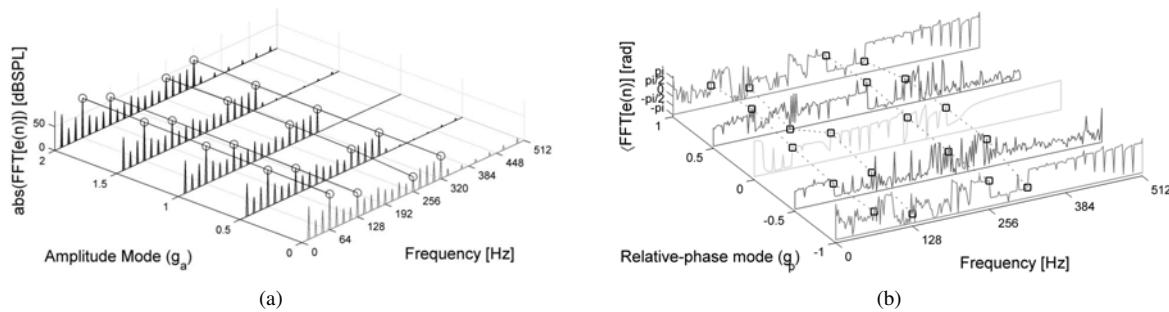


Figure 7. Control actions over the 2.0, 4.0, 8.0 and 10.0 integer orders of the engine disturbance when rotating at 1920 RPM, at the passenger's position: (a) Amplitude modes; (b) Relative-phase modes

Concerning the relative-phase modes, only the 4.0 engine order was near the requested relative-phase values when modes $g_p = \{-1.0, 1.0\}$ were implemented, with a slight difference of 0.07 rad between the expected and the measured values. These relative-phase modes are especially difficult of accomplishing in MIMO control systems, as they require large amounts of power, thus inevitably influencing other SAP outputs.

SQ Analysis

Table 4 shows the SQ results with respect to the amplitude operation modes applied at both positions. As expected, the amplitude modes resulted in the modification of the perceived Loudness, according to the amplification or reduction of the targeted components. Roughness, on the contrary, was kept approximately the same for all the amplitude operation modes, except the $g_a = 0.0$ mode, when it is observed an increase of the auditory phenomenon. It is due, arguably, to the other interactions among the remaining engine orders in the disturbance.

Table 4. Amplitude modes and Sound Quality assessment for Example 2

| Position | Ord. | $g_a = 2.0$ | | | | $g_a = 1.5$ | | | | $g_a = 1.0$ | | | | $g_a = 0.5$ | | | | $g_a = 0.0$ | | | |
|-----------|------|-------------|-------|-------|-------|-------------|-------|-------|------|-------------|-------|-------|------|-------------|-------|-------|--|-------------|-------|-------|--|
| | | dB | sones | asper | | dB | sones | asper | | dB | sones | asper | | dB | sones | asper | | dB | sones | asper | |
| Driver | 2.0 | 79.20 | 3.97 | 0.13 | 76.10 | 2.79 | 0.03 | 72.53 | 2.26 | 0.02 | 68.33 | 1.82 | 0.09 | 64.03 | 1.46 | 0.24 | | | | | |
| | 4.0 | 55.18 | | | 52.61 | | | 49.48 | | | 46.50 | | | 44.98 | | | | | | | |
| | 8.0 | 44.85 | | | 40.17 | | | 37.19 | | | 37.11 | | | 33.32 | | | | | | | |
| | 10.0 | 52.73 | | | 43.26 | | | 42.91 | | | 43.68 | | | 41.21 | | | | | | | |
| Passenger | 2.0 | 82.59 | 4.99 | 0.08 | 80.84 | 4.26 | 0.05 | 79.01 | 3.79 | 0.02 | 77.07 | 3.36 | 0.04 | 74.88 | 2.98 | 0.20 | | | | | |
| | 4.0 | 58.52 | | | 57.50 | | | 55.96 | | | 53.76 | | | 50.70 | | | | | | | |
| | 8.0 | 44.70 | | | 45.14 | | | 43.65 | | | 40.35 | | | 30.75 | | | | | | | |
| | 10.0 | 55.41 | | | 51.28 | | | 49.33 | | | 48.37 | | | 47.72 | | | | | | | |

The SQ results when relative-phase operation modes of the SF-cFxLMS are reported in Tab. 5. It can be observed that

Roughness is drastically modified when relative-phase modes are applied over the targeted narrowband components, at both positions. The observed undesired result is the alteration of Loudness, as this psychoacoustic parameter is insensitive to relative-phase manipulations. Modes $g_p = \{-0.5, 0.5\}$ do not significantly alter the perceived Loudness (max. 0.86 sone at the driver's position and max. 0.32 sone at the passenger's position). Modes $g_p = \{-1.0, 1.0\}$ do not significantly alter the Loudness at the driver's position (max. 0.65 sone), but they do alter it in a perceivable form at the passenger's position (max. 1.39 sone).

Table 5. Relative-phase modes and Sound Quality assessment for Example 2

| Position | Ord. | $g_p = 1.0$ | | | $g_p = 0.5$ | | | $g_p = 0.0$ | | | $g_p = -0.5$ | | | $g_p = -1.0$ | | |
|-----------|------|-------------|------|-------|-------------|------|-------|-------------|------|-------|--------------|------|-------|--------------|------|-------|
| | | rad | sone | asper | rad | sone | asper | rad | sone | asper | rad | sone | asper | rad | sone | asper |
| Driver | 2.0 | -1.49 | 1.61 | 0.33 | 2.29 | 2.70 | 0.35 | 0.46 | 2.26 | 0.02 | -2.29 | 3.12 | 0.17 | -1.50 | 1.61 | 0.33 |
| | 4.0 | 2.88 | | | 3.13 | | | 1.44 | | | -2.95 | | | 2.89 | | |
| | 8.0 | 1.29 | | | 2.50 | | | 0.98 | | | 1.05 | | | 1.36 | | |
| | 10.0 | -1.17 | | | 1.77 | | | 1.15 | | | 1.09 | | | -1.18 | | |
| Passenger | 2.0 | 0.42 | 2.40 | 0.36 | 1.82 | 3.69 | 0.29 | 0.57 | 3.79 | 0.02 | -0.17 | 3.47 | 0.17 | 0.42 | 2.40 | 0.36 |
| | 4.0 | -1.40 | | | -3.10 | | | 1.67 | | | 0.27 | | | -1.41 | | |
| | 8.0 | 1.22 | | | 2.06 | | | 1.42 | | | 0.97 | | | 1.40 | | |
| | 10.0 | -1.19 | | | 1.21 | | | 1.66 | | | 1.68 | | | -1.18 | | |

3.2.1 Impulsive Event

The last simulation scenario demonstrates the use of the forgetting factor ρ in the implementation of a robust MIMO SF-cFxLMS system, when impulsive events are present in the incoming disturbance. The control algorithm is implemented by using the set of constrainings, i.e. δ -factors, given for the amplitude operation modes (see Tab. 3). Figure 8 shows the time histories of the reduction mode $g_a = 0.0$ applied over the targeted set of narrowband components of the primary disturbance, i.e. 2.0, 4.0, 8.0 and 10.0 engine orders, at both the driver's and passenger's positions.

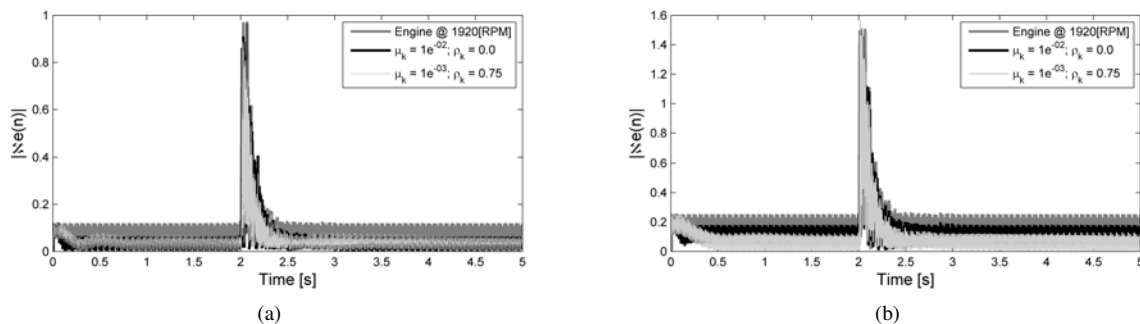


Figure 8. Comparison of two time histories for illustrating the use of the forgetting factor ρ : (a) Driver's position; (b) Passenger's position

The implementation of the proposed control algorithm without forgetting factors provides a fast initial convergence, as it can be evidenced in Fig. 8 at both positions. However, after emergence of the impulsive event, the convergence period is larger than when using forgetting factors and smaller step-sizes (μ) of the adaptive algorithm. In the former case, the *re-convergence* of the algorithm takes *inherently* in account all the time history of the control system, as a consequence of merely changing the expectation operator in Eq. 1 by its instantaneous value. In contrast, the forgetting factor ρ *weights the recent data*, i.e. the last τ data blocks, as stated in Eq. 9, resulting in a less noisy gradient estimator, thus becoming more robust to recent, unexpected incoming events. It can be evidenced in Fig. 8 that, when forgetting factors of $\rho = 0.75$ are implemented at both positions, the “re-convergence” of the system is faster and more accurate than in the former setup. Hence, it is demonstrated through this Scenario that the proposed robustness tool is also compatible with the δ -constrainings for each narrowband component being controlled.

4. CONCLUSION

This paper presents a multiple-input, multiple-output adaptive algorithm for controlling the sound quality of a multi-harmonic disturbance, based on both the amplitude and relative-phase of its narrowband components. Concerning automotive active noise control applications, different auditory perceptions of the engine disturbance at several relevant positions inside a passenger's cavity can be preferred, instead of globally reducing the disturbance, which could lead to perceive other undesired vibroacoustic phenomena. In view of such a goal, we present a decentralized MIMO control strategy, which also constrains the controller effort in a order-by-order form, by deriving a modified cost function based

on the single-input, single-output SF-cFxLMS' one, hence aiming at reducing the impact of the performed control actions at a specific location on the other sensor-actuator pairs in the system.

The so-called constrained MIMO SF-cFxLMS algorithm, presented in this paper, is extensively simulated by using a synthesized, stationary internal combustion engine noise and pure-delay primary and secondary transfer paths. Two positions inside a hypothetical cavity being radiated by the primary disturbance were simultaneously controlled, and the resulting time histories were assessed in terms of their final spectra values and relevant SQ metrics such as Loudness and Roughness. Features of the proposed algorithm such as independent amplitude and/or relative-phase control of the narrowband components without distorting other components, fast and stable convergence process and effort constraints that avoid cross-action effects over other SAP in a cavity, lead to obtain proposed control and SQ targets over the disturbance. Furthermore, inclusion of forgetting factors in the proposed adaptive algorithm improve robustness of the system face to impulsive events, which leads to swiftly re-converge to the desired control output, even when using effort constraining factors in the MIMO control system.

5. ACKNOWLEDGEMENTS

The authors gratefully acknowledge the financial support of the São Paulo Research Foundation - FAPESP and the Brazilian National Council for Scientific and Technological Development - CNPq.

REFERENCES

- Cabell, R.H. and Fuller, C.R., 1999. "A principal component algorithm for feedforward active noise and vibration control". *Journal of Sound and Vibration*, Vol. 227, pp. 159 – 181.
- Daniel, P. and Weber, R., 1997. "Psychoacoustical roughness: implementation of an optimized model". *Acustica - Acta Acustica*, Vol. 83, pp. 113 – 123.
- de Diego, M., Gonzalez, A., Ferrer, M. and Piñero, G., 2004. "Multichannel active noise control system for local spectral reshaping of multifrequency noise". *Journal of Sound and Vibration*, Vol. 274, pp. 249 – 271.
- Elliott, S.J. and Boucher, C.C., 1994. "Interaction between multiple feedforward active control systems". *IEEE Transactions on Speech and Audio Processing*, Vol. 2, pp. 521 – 530.
- Fastl, H. and Zwicker, E., 2007. *Psychoacoustics: Facts and Models*. Springer-Verlag.
- Gonzalez, A., de Diego, M., Ferrer, M. and Piñero, G., 2006. "Multichannel active noise equalization of interior noise". *IEEE Transactions on Audio, Speech and Language Processing*, Vol. 14, No. 1, pp. 110 – 122.
- Janssens, K., Ahrens, S., Bertrand, A., Lanslots, J., Van de Ponselee, P., Vecchio, A. and Van der Auweraer, H., 2007. "An on-line, order-based roughness algorithm". In *SAE International*. 07NVC-173, pp. 1 – 9.
- Jeon, H.J., Chang, T.G., Yu, S. and Kuo, S.M., 2011. "A narrowband active noise control system with frequency corrector". *IEEE Transactions on Audio, Speech and Language Processing*, Vol. 19, No. 4, pp. 990 – 1002.
- Kuo, S.M. and Morgan, D.R., 1996. *Active Noise Control Systems: algorithms and DSP implementations*. Wiley.
- Kuo, S.M., Yenduri, R.K. and Gupta, A., 2008. "Frequency-domain delayless active sound quality control algorithm". *Journal of Sound and Vibration*, Vol. 318, pp. 715 – 724.
- Mosquera-Sánchez, J.A., 2012. *Active Structural Acoustic Control: Design, Simulation and Sound Quality Analysis (in Portuguese)*. Master's thesis, São Carlos School of Engineering - University of São Paulo.
- Mosquera-Sánchez, J.A. and Oliveira, L.P.R., 2012. "An adaptive controller for amplitude and relative phase of periodic disturbance". In *Proceedings of ISMA2012*.
- Oliveira, L.P.R., Stallaert, B., Desmet, W., Swevers, J. and Sas, P., 2005. "Optimisation strategies for decentralized ASAC". In *Proceedings of Forum Acusticum*. Budapest, pp. 875 – 880.
- Oliveira, L.P.R., Stallaert, B., Janssens, K., Van der Auweraer, H., Sas, P. and Desmet, W., 2010. "NEX-LMS: A novel adaptive control scheme for harmonic sound quality control". *Mechanical Systems and Signal Processing*, Vol. 24, pp. 1727 – 1738.
- Pasco, Y., Robin, O., Bélanger, P., Berry, A. and Rajan, S., 2011. "Multi-input multi-output feedforward control of multi-harmonic gearbox vibrations using parallel adaptive notch filters in the principal component space". *Journal of Sound and Vibration*, Vol. 330, pp. 5230 – 5244.
- Pressnitzer, D. and McAdams, S., 1999. "Two phase effects in roughness perception". *Journal of the Acoustical Society of America*, Vol. 105, pp. 2773 – 2782.
- Rees, L.E. and Elliott, S.J., 2006. "Adaptive algorithms for active sound-profiling". *IEEE Transactions on Audio, Speech and Language Processing*, Vol. 14, No. 2, pp. 711 – 719.
- Sun, X. and Meng, G., 2006. "LMS algorithm for active noise control with improved gradient estimate". *Mechanical Systems and Signal Processing*, Vol. 20, pp. 920 – 938.

RESPONSIBILITY NOTICE

The authors are the only responsible for the printed material included in this paper.